R. & M. No. 3290

MINISTRY OF AVIATION

AERONAUTICAL RESEARCH COUNCIL
REPORTS AND MEMORANDA

Free-Flight Measurements of Pressure Distribution at Transonic and Supersonic Speeds on Bodies of Revolution Having Parabolic Afterbodies

By C. KELL

LONDON: HER MAJESTY'S STATIONERY OFFICE
1962
PRICE: 9*s*. 6*d*. NET

Free-Flight Measurements of Pressure Distribution at Transonic and Supersonic Speeds on Bodies of Revolution Having Parabolic Afterbodies

By C. Kell

Communicated by the Director-General of Scientific Research (Air), Ministry of Supply

*Reports and Memoranda No. 3290**
April, 1958

Summary. Free-flight measurements have been made of the pressure distributions over a series of related afterbodies attached to a common cone-cylinder body of revolution. The Mach number range covered was from 0·9 to 1·5 and the Reynolds number range from 31 to 65 × 10^6.

The experimental results were in reasonable agreement with theoretical values calculated by the method of characteristics and confirm the usefulness of the supersonic similarity law as a means of predicting drag.

Measurements of base pressure were qualitatively in agreement with estimates but quantitatively the agreement was not good. Limitations in the experimental technique and in certain cases the occurrence of flow separation are jointly held responsible for the discrepancies. The measured boundary-layer displacement thicknesses on the afterbody were in good agreement with estimated values.

1. *Introduction.* During recent years the problem of predicting the nature of the flow on axi-symmetric afterbodies and the relation between the afterbody flow and the base pressure has been of increasing interest to the many workers involved in the design of aircraft and guided missiles. In Ref. 1 a theoretical treatment of the pressures over a series of parabolic afterbodies was made by Fraenkel and the purpose of the present report is to give the results obtained by experiments made on models having substantially the same shapes and dimensions as those dealt with by Fraenkel. This report thus forms part of the complete theoretical and experimental investigation described in Ref. 1.

The experimental results were obtained by means of the free-flight technique: the models were flown near sea-level over the Mach number range 0·9 to 1·5 and the Reynolds numbers were substantially the same as for the theoretical treatment, *i.e.*, between 31 and 65 millions based on body total length. The only significant difference between the theoretical and experimental bodies was the presence of stabilizing fins on the latter.

* Previously issued as R.A.E. Report No. Aero. 2605—A.R.C. 20,433.

2. *Description of Models and Technique.* The basic body dealt with in Ref. 1 was 4·95 in. diameter, 39·60 in. (8 diameters) long, with a conical nose 19·80 in. (4 diameters) long. The total nose-plus-body length was the same for the experimental work but instead of the sharp corner at the junction of the nose and body a radius was formed to reduce the risk of flow separation occurring. The radius was such that the curve was tangential to the parallel body at a station one diameter aft of the theoretical intersection of the conical and parallel surface, where the original corner was formed, and was also tangential to the conical surface at a station nearly one diameter forward of the corner. Thus, although the overall length of the models was the same as in Ref. 1 the parallel portion was one diameter shorter.

Three basic types of afterbody were tested; these were parabolic in shape, tangential at the forward end to the surface of the parallel body. The three shapes of afterbody were defined by the ratio $t = R/L$, where R was the maximum body radius and L the length of the afterbody when considered to continue to a point (Fig. 1). Each of the three basic shapes was further broken down by cutting the afterbody at one of three stations so as to produce three afterbodies for a given profile, each having a different ratio of base radius r to maximum body radius R. The values chosen for t were the same as in Ref. 1, *i.e.*, 0·1, 0·1414 and 0·2, and afterbodies having values of r/R equal to 0·6, 0·8 and 0·9 were tested for each of these values of t (Fig. 1).

Four stabilizing fins, in a cruciform arrangement, were fitted to the parallel portion of the body with their root leading edges 11·65 in. (2·35 diameters) forward of the body-afterbody junction (*see* Figs. 1 and 2). The leading edge of each fin was swept back 45 deg, the root chord was 6 in. and the tip chord 1 in. Both the leading and trailing edges were chamfered 0·5 in. and the fin thickness was a constant 0·128 in. giving root and tip thickness/chord ratios of 2·1 and 12·8 per cent respectively.

Near the trailing edge of one pair of opposing fins, slot aerials were fitted; one of these aerials received a radio-doppler signal radiated from the ground station and the other re-transmitted the signal after it had been fed to the Doppler transponder carried within the model. From the records obtained from Doppler equipment the velocity and longitudinal acceleration were determined. Similar slot aerials were fitted to the remaining two stabilizing fins and these radiated the signal from the 465 mc/s multi-channel telemetering equipment also carried within the model.

Surface-pressure measurements were made at a series of stations along the rear of the parallel body and along the afterbody itself. At each station there were two pressure-measuring points located diametrically opposite each other. There were thus two lines of pressure points extending from a station just aft of the fin trailing edges and arranged at 45 deg to the fins so as to reduce fin interference to a minimum. The positions of these measuring stations are shown in Fig. 3.

On all the models two measurements of base pressure were made, one measuring point being at the centre of the base and the other at 0·69 of the base radius from the centre. An attempt was also made on three of the models to measure the velocity profile in the afterbody boundary layer by means of a pitot comb. These measurements were made as far aft on the model as was practicable but some distance ahead of the actual base, owing to the necessity for leaving an uninterrupted finish near the rear to allow the boost-motor cup to be fitted. The three models on which velocity profiles were measured were those having $t = 0·1$ and r/R equal to 0·6, 0·8 and 0·9 respectively. Fig. 3 shows the form of the pitot comb and its position on each model. Each of the comb pitots was formed from hypodermic tube of 2 mm outside diameter with the open end tapered to give a sharp edge and flattened in one plane so as to give a maximum opening of 0·04 in. normal to

the surface of the body. The tubes were connected to the pressure transducers in the model in such a way that they recorded the difference between pitot pressure in the boundary layer and free-stream pitot pressure, the latter pressure being supplied by a pitot probe mounted at the extreme nose of the model (Fig. 1).

In addition to the pressure transducers each model was fitted with a longitudinal accelerometer and the results from this transducer were combined with those from radio-Doppler to give a measurement of overall drag.

The models were boosted to a maximum speed of about $M_\infty = 1{\cdot}5$ by means of a single 5 in. L.A.P. rocket motor and were arranged to separate from the boost at the completion of burning. They then coasted down through the Mach number range to a minimum Mach number of about $0{\cdot}9$. Fig. 2a shows one of the models attached to the boost. Some difficulty was experienced during the boosting phase because the pressures around the boost cup affected the afterbody pressures and these tended to exceed the calibrated range of the instruments for a short time. An attempt to reduce these effects by means of a cage-like structure for the cup (Fig. 2a) helped to improve matters but was not a complete answer to the problem.

The methods of obtaining telemetered information, velocity, acceleration and height during the flight were the standard methods already described fully in Ref. 2. Data on the atmospheric pressure, temperature and wind velocity at the appropriate flight conditions were obtained in the usual way from meteorological measurements made at the range-head.

3. *Results.* 3.1. *Pressure Distribution.* In Figs. 4, 5 and 6 pressure coefficients deduced from the measurements are plotted against free-stream Mach number for each of the longitudinal stations. The results quoted are means of the pairs of values recorded at each station. There was a gap in the transonic results for the long afterbody ($r/R = 0{\cdot}6$) with $t = 0{\cdot}1$, and no results were obtained for the long afterbody with $t = 0{\cdot}1414$; in both experiments this was due to instrument failures which occurred during the flight.

The results have been replotted in Figs. 7, 8 and 9 to show the variation of pressure along the afterbody at given values of Mach number. In these figures the theoretical pressure-distribution curves, as given by Fraenkel, are also plotted; two curves are shown, one with, and the other without, the effect of boundary layer. It is clear that the measured afterbody pressure coefficients are generally higher than theory would suggest. It would be necessary to apply a factor of two or three to the estimated boundary-layer effect in order to account for the discrepancy by this means alone. In fact the evidence from the pitot-comb measurements (Section 3.4) confirms that the thickness of the boundary layer is close to that predicted by Fraenkel.

There is a fair amount of scatter between the points for differing afterbody length (t constant) but little systematic variation.

The results plotted in Figs. 7, 8 and 9 include pressures measured on the parallel part of the body, $4{\cdot}45$ in. forward of the afterbody shoulder. These pressures are substantially different from those predicted by Fraenkel but it seems likely that the discrepancy is a localised one, caused by expansion waves over the rear of the stabilising fins. It is suggested that this discrepancy can be neglected when comparing the afterbody pressures with theory.

The measured values of pressure on the base, which are discussed in more detail in the next section, have been included on Figs. 7, 8 and 9. It is seen that in most cases the base pressure is lower than the final pressure on the afterbody, that is to say, the flow makes a further expansion

over the rear edge. Thus it is not possible to account for the general discrepancy between theory and experiment in terms of higher pressure in the real base flow extending forwards over the afterbody through the boundary layer.

As the value of t increases, and more particularly with the longer afterbodies, the pressures near the end of the afterbody become more negative and the pressure jump at the base tends to change sign. With $t = 0{\cdot}2$ (Fig. 9), the pressure jump is still negative for the short afterbody but positive for both medium and long afterbodies. For this last case, there is some evidence (*see* Section 3.2) that, as a result of this trend, flow separation occurred on the afterbody at low supersonic M. This leads to a spread of pressure upstream from the base, increasing the discrepancy between experiment and theory.

The comparison, made in Ref. 1, between the exact and linearised solutions is reproduced in Fig. 10a and the corresponding experimental points are included. Fraenkel pointed out that the principal failing of the quasi-cylinder result was its inability to show the recompression towards the tail which the other methods predicted. The experimental points clearly indicate this recompression and, as we should expect, the greatest error between theory and experiment occurs when the quasi-cylinder result is considered. A similar result is shown in Fig. 10b where C_D is compared for theory and experiment. In this case the experimental values are those obtained by integrating the measured normal pressures.

3.2. *Base Pressure.* Two measurements of base pressure were made on each model; one measuring point was at the centre of the base, the other $0{\cdot}69\ r$ out from the centre. No systematic difference between readings at the two points was found but, where random differences have occurred, mean values have been used in presenting the results.

In Fig. 11 the ratio p_b/p_∞ has been plotted against free-stream Mach number. Considered in groups having fixed values of t, the curves show that there was a progressive reduction in base pressure as the afterbody was reduced in length, the lowest value occurring when the afterbody was removed altogether.

In Ref. 3 a method is proposed whereby base-pressure estimates may be made for two- and three-dimensional bodies based on an analogy with the pressure rise required to separate a boundary layer. This analogy indicates that one would expect the base pressure to be closely related to the angle of the afterbody trailing edge and in Ref. 4 Socha presents curves showing this theoretical relationship and indicating the extent to which existing experimental data confirm the theory. Most of the experimental results for conical afterbodies to which he had access were at Mach numbers greater than $1{\cdot}5$ but they did indicate that there was fair agreement for angles up to 5 deg.

The results from the present tests refer to parabolic afterbodies but this should not affect the argument on which the theoretical analogy is based, the trailing-edge angle β being the angle on which base pressure would be dependent. In Fig. 12 the present experimental results are plotted together with the predicted curves suggested in Ref. 4. The base-pressure coefficient and Mach number in this figure relate to the pressure p_1 and Mach number M_1 on the surface of the afterbody immediately forward of the base; these were deduced from the measured pressure distributions.

The plot of experimental results in Fig. 12 does show that there is a dependence on angle β, but a close approach to quantitative agreement with the theory occurs only at the highest Mach numbers of the tests, *i.e.*, when $M_1 \approx 1{\cdot}6$. Below this Mach number the dispersion of the results increases, suggesting that factors other than β are becoming important. For the case $\beta = 0$ deg, *i.e.*, no

afterbody, the measured pressures are lower than predicted and this is consistent with experimental results collected in Ref. 4.

As the afterbody angle progressively increases, a condition is eventually reached where the boundary layer separates and the shock at the corner of the base moves forward to a point on the afterbody where equilibrium is again achieved. On the basis of the analogy of Ref. 3 this implies that a boundary exists which sets an upper limit to the base-pressure coefficient to be expected for a given value of M_1. This predicted boundary is shown in Fig. 12. The experimental results for the afterbodies with the highest values of β (10·1 deg and 14·2 deg) do indeed suggest that separation occurred on these models: the shape of the curves in Fig. 12 is similar to that of the predicted curve. Again however quantitative agreement is poor, particularly in the case of the afterbody where $\beta = 14{\cdot}2$ deg. One would expect to detect a separation from the surface pressure measurements but this is difficult because of the limited number of measuring points. There is therefore no way of knowing how far the differences between Fraenkel's predictions and our measurements are due to limitations in the theory or to separation effects. Nevertheless, Fig. 9a indicates that for the model where $\beta = 14{\cdot}2$ ($t = 0{\cdot}2$, long afterbody) the recorded pressures near the trailing edge are higher than the experience with the other afterbodies would suggest and this may well be due to flow separation.

3.3. *Drag Measurements.* The total drag of each model was measured throughout the Mach number range and the results are shown plotted in Fig. 13. Because of the reduced accuracy of measurement at subsonic speeds it would be wrong to draw firm conclusions about the relative drags of the different afterbodies in this part of the range; although the general level is probably correctly indicated.

In Fig. 14 an attempt has been made to show the drag breakdown for each afterbody. Base drag was estimated from the results of the measured base pressure and pressure drag from an integration of the afterbody surface pressures when resolved along the line of flight. Skin-friction drag was estimated on the basis of the flat-plate values given by Fraenkel (Ref. 1). The total length of the model was used in choosing values of C_f for this purpose.

By subtracting the base drag from the total drag of the model which had no afterbody, an estimate was obtained for the forebody-plus-fin drag. Using this value of forebody drag, the drag of each afterbody itself was determined and these results are also plotted in Fig. 14. It is seen that the total afterbody drag obtained by this method is consistently higher than that given by the sum of the estimated base, pressure and friction drags. It is noted that the afterbody drag as obtained from differences is sensitive to error in the estimation of forebody-plus-fin drag, and this in turn depends critically upon the accuracy of measurement of base drag on the model without afterbody, where the base drag amounts to some 50 per cent of total drag. If we assume an error of $\pm$ 3 per cent in the measurement of total drag on the basic model and $\pm$ 3 per cent in the measurement of base pressure, then we may have as much as 9 per cent error in the total forebody drag; this is sufficient to account for the discrepancy between the two methods of estimation of afterbody drag.

In Ref. 1 Fraenkel has shown the extent to which a similarity law allows the afterbody wave-drag results to be collapsed. In Fig. 15 the theoretical results from Ref. 1, for which allowance for boundary layer has been made, are plotted according to the similarity law together with the estimates of these values obtained from the free-flight experiments. It has been seen that the recorded values of afterbody surface pressures are, in general, greater than predicted. The experimental values of $C_D(X/R)^2$ are correspondingly lower by about 10 per cent as Fig. 15 shows.

The good collapse of results (Fig. 15) suggests that the similarity law provides an accurate means for drag estimation when the afterbody flow is not separated. The low-drag points associated with model 7 are indicative of possible separation effects.

3.4. *Boundary-Layer Measurements.* In Fig. 16, the measured boundary-layer profiles for models Nos. 1 and 3† are presented. When estimating the velocity ratio u/u_1 from the total pressures it was assumed that the static pressure was constant across the boundary layer.

An attempt was made to determine the values of the constants given in the expression for boundary-layer profile on which Fraenkel, in Ref. 1, based his estimates but it was clear that the limited number of measurements and the limits in the accuracy of the telemetered results made this approach unreliable and the attempt was abandoned.

In Fig. 17 the velocity ratio u/u_1 is plotted against the thickness ratio y/δ for the two models and a comparison made with the power law $u/u_1 = (y/\delta)^n$. The best mean curve of the results corresponds to a variation in which the power is somewhere between 1/7 and 1/9. Assuming the law $u/u_1 = (y/\delta)^{1/8}$ the displacement thickness δ^* was determined from the curves presented by Cope, Ref. 5, and the resulting values compared in Fig. 18 with those suggested by Fraenkel. Good agreement was obtained between experiment and theory and this suggests that the discrepancy between the theoretical and experimental values of afterbody surface pressures was not due to errors in the estimation of boundary-layer thickness.

4. *Conclusions.* The measured afterbody pressure coefficients were generally higher than those calculated by the exact characteristics method, the difference being of the order of 10 per cent. The trends indicated by theory were in good agreement with those measured and in particular the usefulness of the supersonic similarity law as a design procedure for estimating afterbody drag has been confirmed.

Measurements of base pressure were in qualitative agreement with estimated values but the quantitative agreement was not good, particularly at low supersonic speeds. Limitations in the experimental technique of base-drag measurements and the occurrence of flow separation in certain cases are jointly held to be responsible for the discrepancies.

The measured boundary-layer thicknesses on the afterbody were in good agreement with those estimated by Fraenkel, suggesting that the discrepancy in pressure distribution could not be attributed to the correction for boundary-layer displacement effects.

---

† Unfortunately one of the pitot instruments failed on model No. 2 and the loss of appropriate pressure measurements so limited the value of the remaining points that the results for this model have not been given.

LIST OF SYMBOLS

C_D	Drag coefficient
C_f	Skin-friction coefficient
C_p	Pressure coefficient
L	Length of afterbody continued to a point
M	Mach number
p	Static pressure
r	Radius of base
R	Maximum radius of body
RN	Reynolds number based on total body length
S_a	Body maximum cross-section area
S_b	Base area
X	Actual length of afterbody
t	Ratio R/L
u	Velocity in boundary layer
u_1	Velocity immediately outside boundary layer
x	Distance from body-afterbody junction (positive aft)
y	Radial distance from surface of body
β	Angle between afterbody trailing edge and axis of model (degrees)
γ	Ratio of specific heats of air—taken as 1·4
δ	Boundary-layer thickness
δ^*	Boundary-layer displacement thickness
$(\ )_b$	Conditions at base
$(\ )_1$	Conditions on afterbody surface immediately forward of base
$(\ )_\infty$	Conditions in free stream

REFERENCES

No.	*Author*	*Title, etc.*
1	L. E. Fraenkel	Calculations of the pressure distributions and boundary-layer development on a body of revolution with various parabolic afterbodies at supersonic speeds. A.R.C. R. & M. 2966. February, 1953.
2	T. Lawrence, J. Swan and C. H. E. Warren.	Development of a transonic research technique using ground-launched rocket-boosted models: Part II—Drag measurements. A.R.C. 14,167. March, 1951.
3	Eugene S. Love	Base pressure at supersonic speeds on two-dimensional airfoils and on bodies of revolution with and without fins having turbulent boundary layers. N.A.C.A. Tech. Note 3819. January, 1957.
4	W. Socha	Analysis of base pressure at supersonic speeds. English Electric Co. Aerodynamics Technical Note No. Ae.95. December, 1955.
5	W. F. Cope	Notes and graphs for boundary layer calculations in compressible flow. A.R.C. C.P. 89. August, 1951.

TABLE 1

Details of Afterbody Dimensions

Model No.	t	r/R	X ins.	S_b/S_a	β deg
1	0·1	0·6	15·654	0·36	7·2
2	0·1	0·8	11·068	0·64	5·1
3	0·1	0·9	7·826	0·81	3·6
4	0·1414	0·6	11·068	0·36	10·1
5	0·1414	0·8	7·826	0·64	7·2
6	0·1414	0·9	5·534	0·81	5·1
7	0·2	0·6	7·826	0·36	14·2
8	0·2	0·8	5·534	0·64	10·1
9	0·2	0·9	3·913	0·81	7·2
10		1·0	0	1·00	0

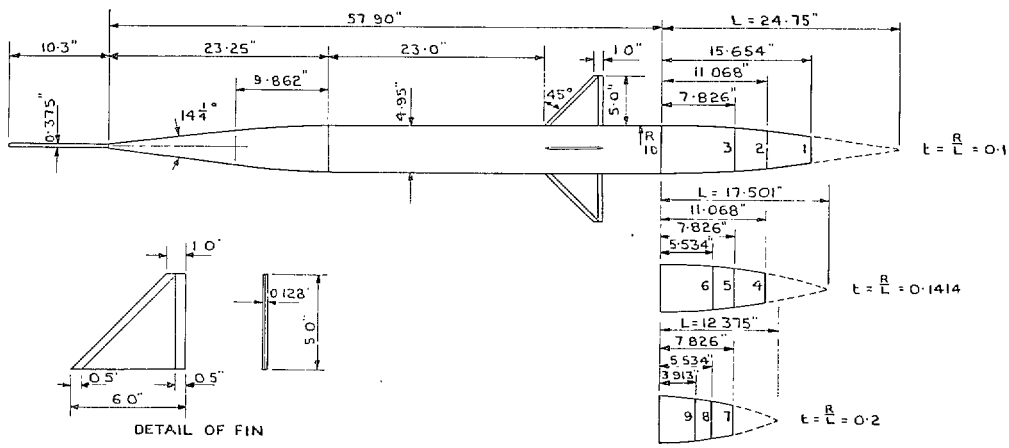

FIG. 1. Layout of test vehicle for afterbody pressure measurements.

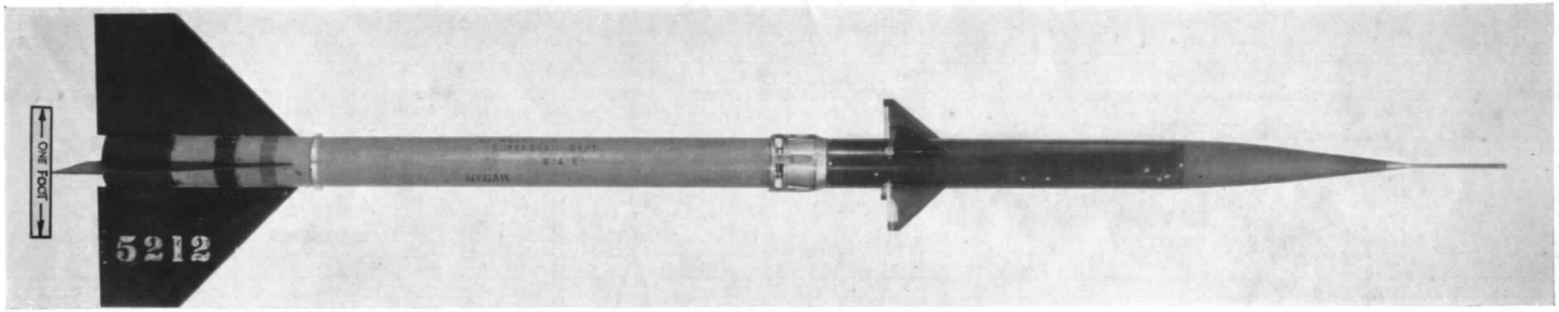

(a) Model mounted on 5-inch L.A.P. boost motor.

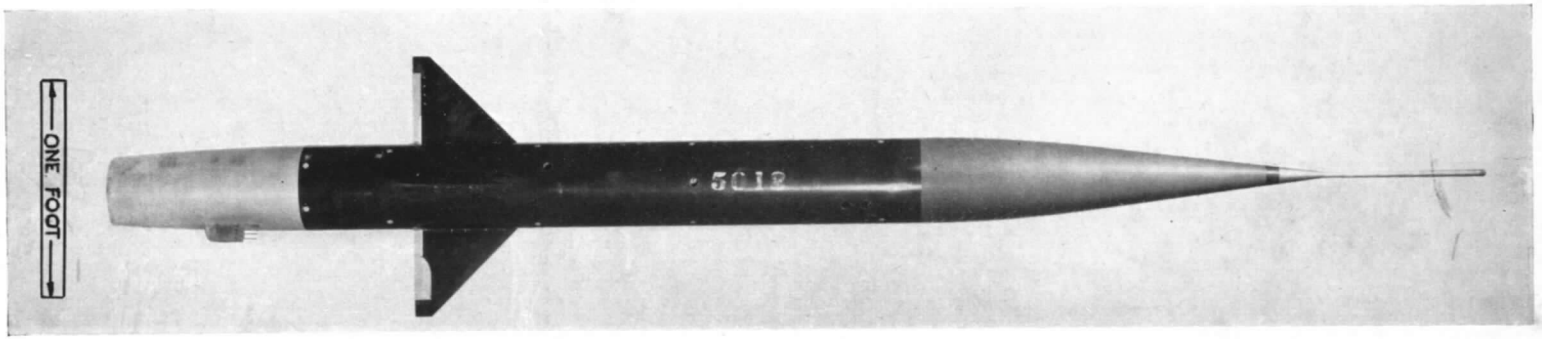

(b) Typical model used for the measurements of afterbody pressures.

FIGS. 2a and b. Typical model, and model-plus-boost arrangement.

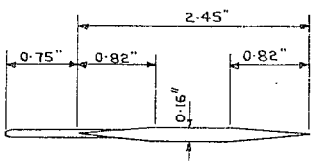

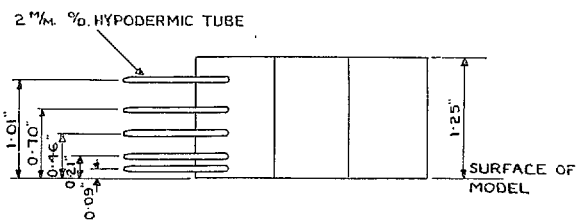

PITOT COMB FOR BOUNDARY PRESSURE MEASUREMENTS.

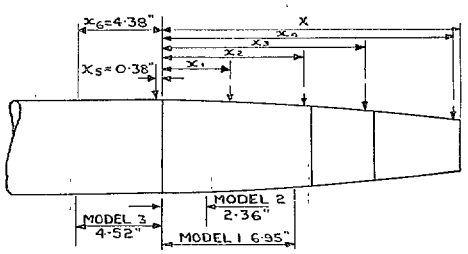

PITOT COMB MEASURING PLANES.

MODEL	R/L	X"	P"	X_1"	X_2"	X_3"	X_4"
1	0·1	15·654	1·485	3·54	7·45	10·69	15·274
2	0·1	11·068	1·980	3·54	7·45	10·69	
3	0·1	7·826	2·227	3·54	7·45		
4	0·1414	11·068	1·485	2·59	5·16	7·45	10·69
5	0·1414	7·826	1·980	2·59	5·16	7·45	
6	0·1414	5·534	2·227	2·59	5·16		
7	0·2	7·826	1·485	1·79	3·54	5·16	7·45
8	0·2	5·534	1·980	1·79	3·54	5·16	
9	0·2	3·913	2·227	1·79	3·54		
10		0	2·475				

STATIC PRESSURE MEASURING POINTS.

FIG. 3. Details and positions of pitot- and static-pressure measuring points.

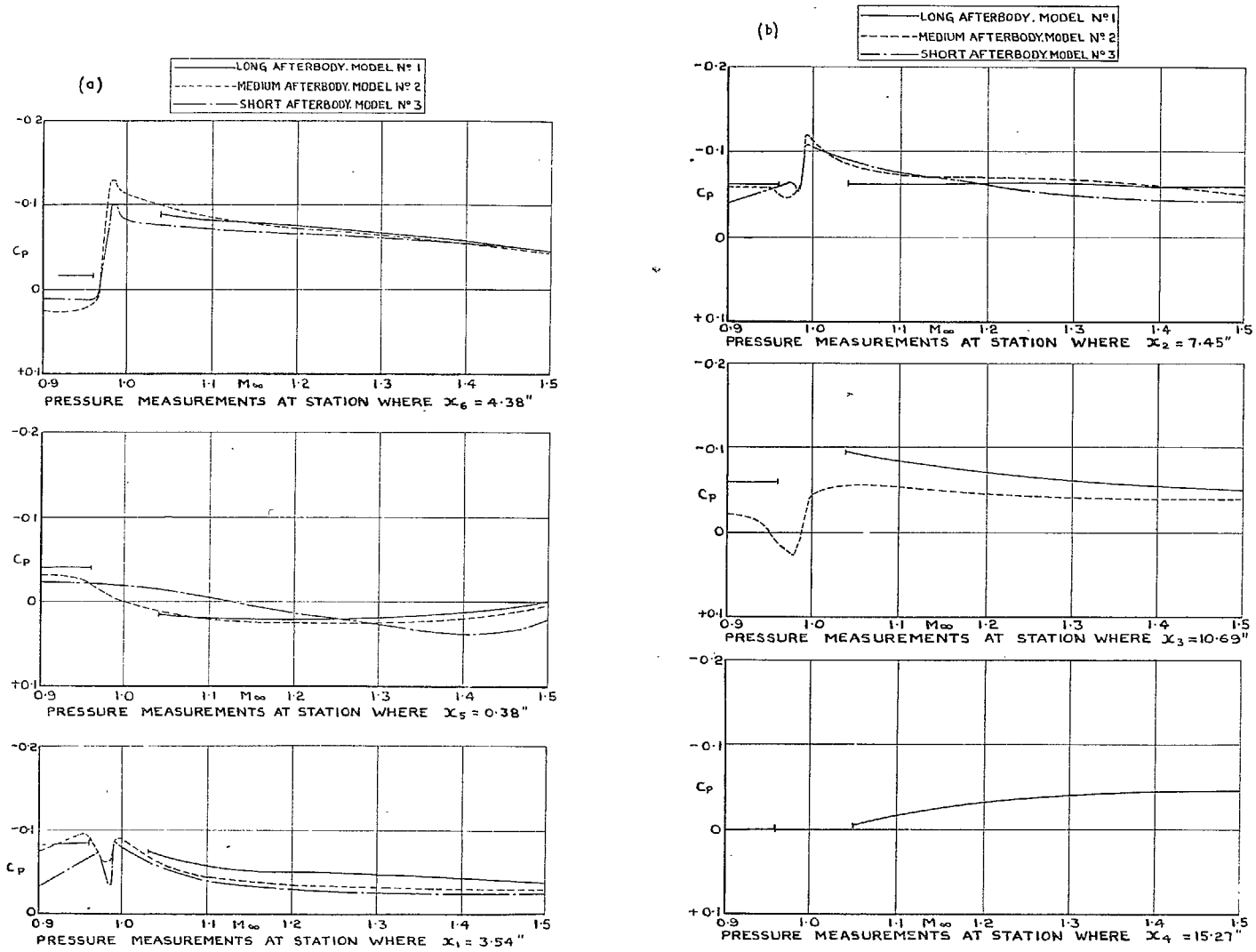

FIGS. 4a and b. Variation of pressure coefficient with Mach number for $t = 0{\cdot}1$.

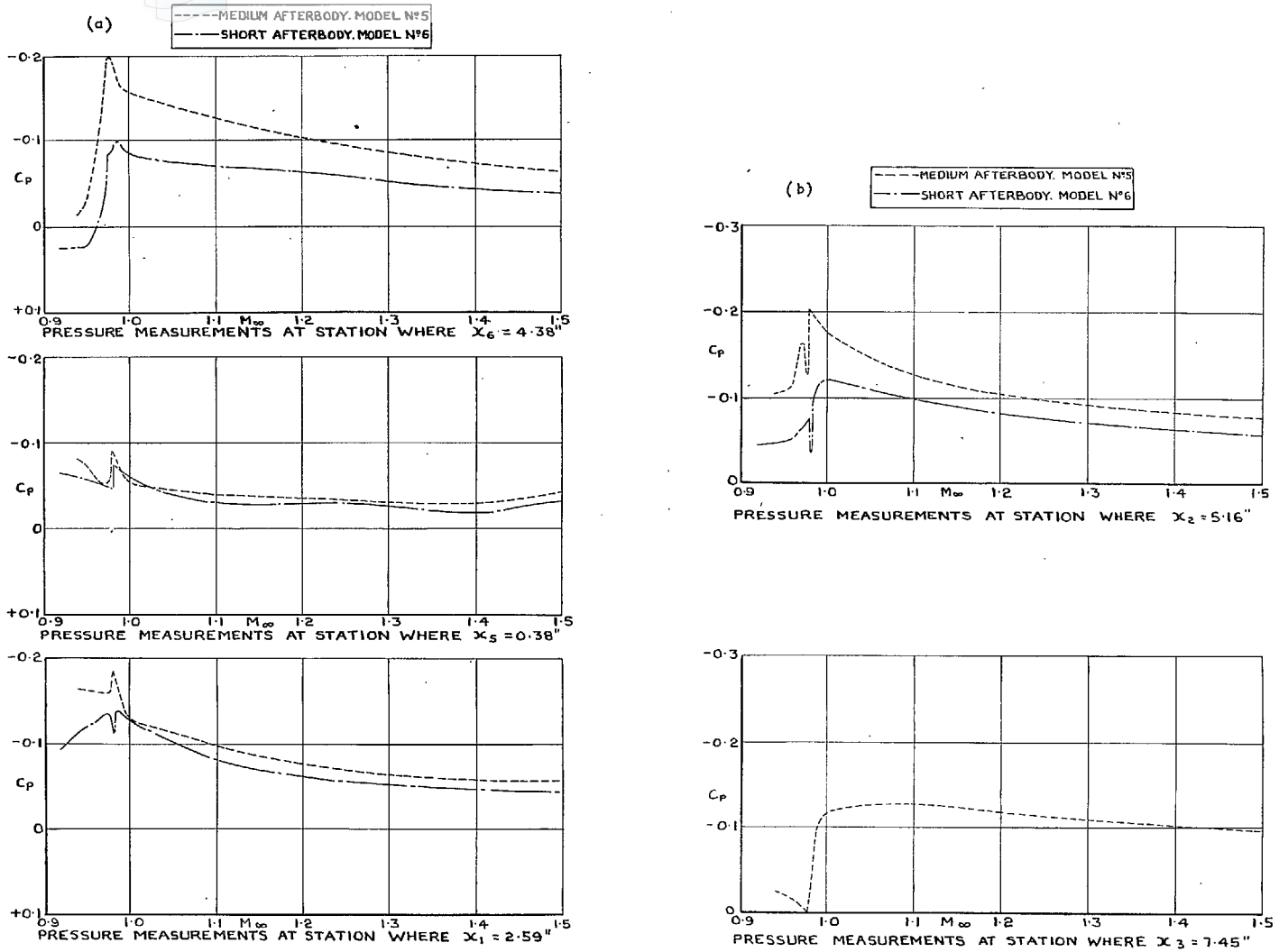

FIGS. 5a and b. Variation of pressure coefficient with Mach number for $t = 0·1414$.

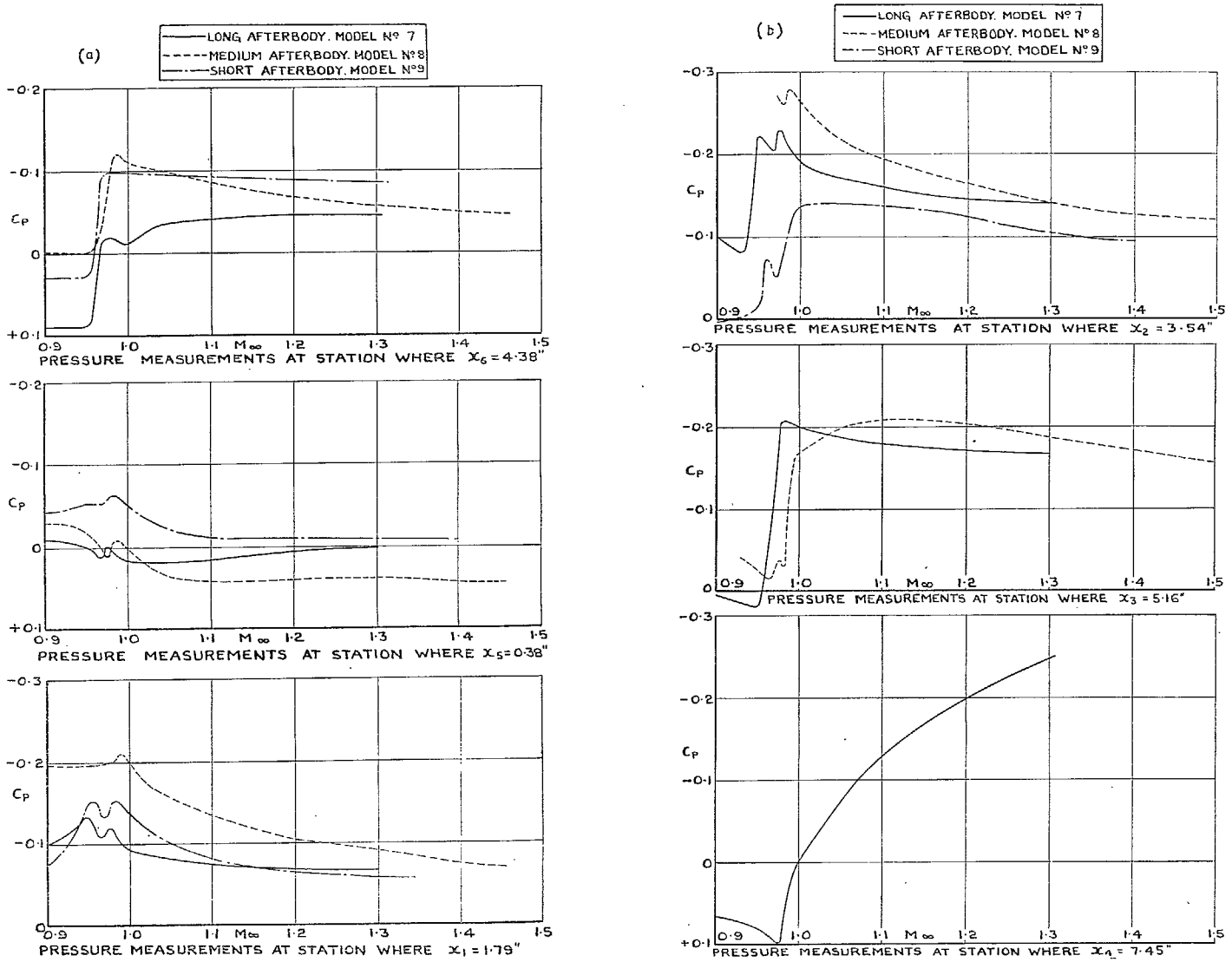

FIGS. 6a and b. Variation of pressure coefficient with Mach number for $t = 0{\cdot}2$.

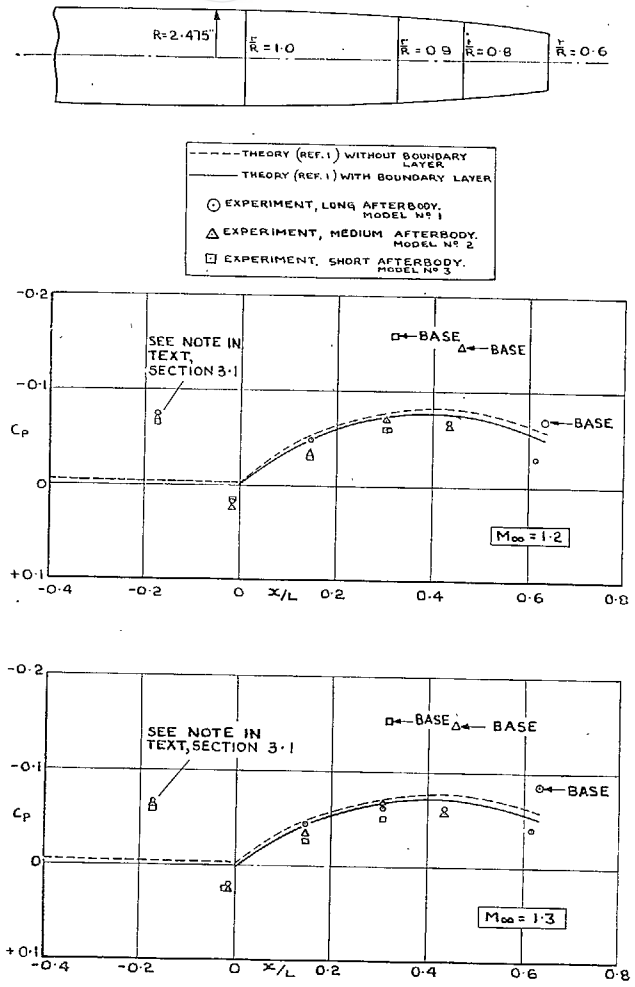

FIG. 7a. Afterbody pressure distribution. $t = 0·1$. $M_\infty = 1·2$ and $1·3$.

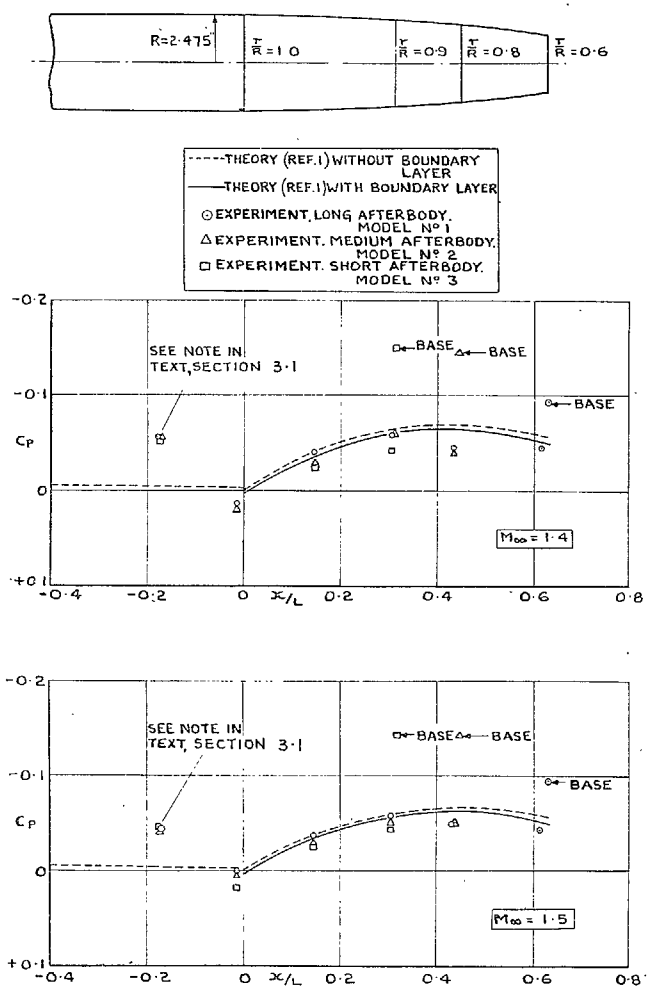

FIG. 7b. Afterbody pressure distribution. $t = 0·1$. $M_\infty = 1·4$ and $1·5$.

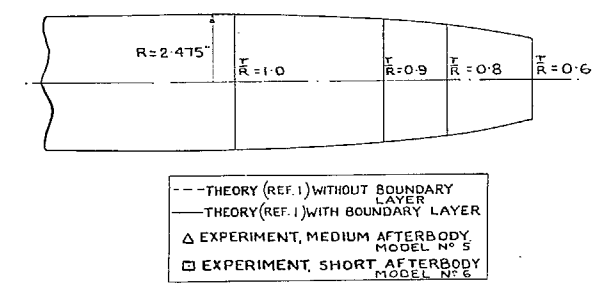

FIG. 8a. Afterbody pressure distribution. $t = 0·1414$. $M_\infty = 1·2$ and $1·3$.

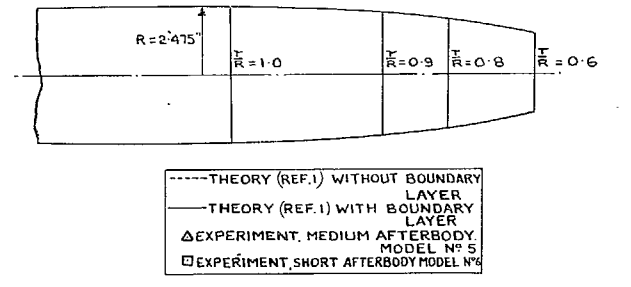

FIG. 8b. Afterbody pressure distribution. $t = 0·1414$. $M_\infty = 1·4$ and $1·5$.

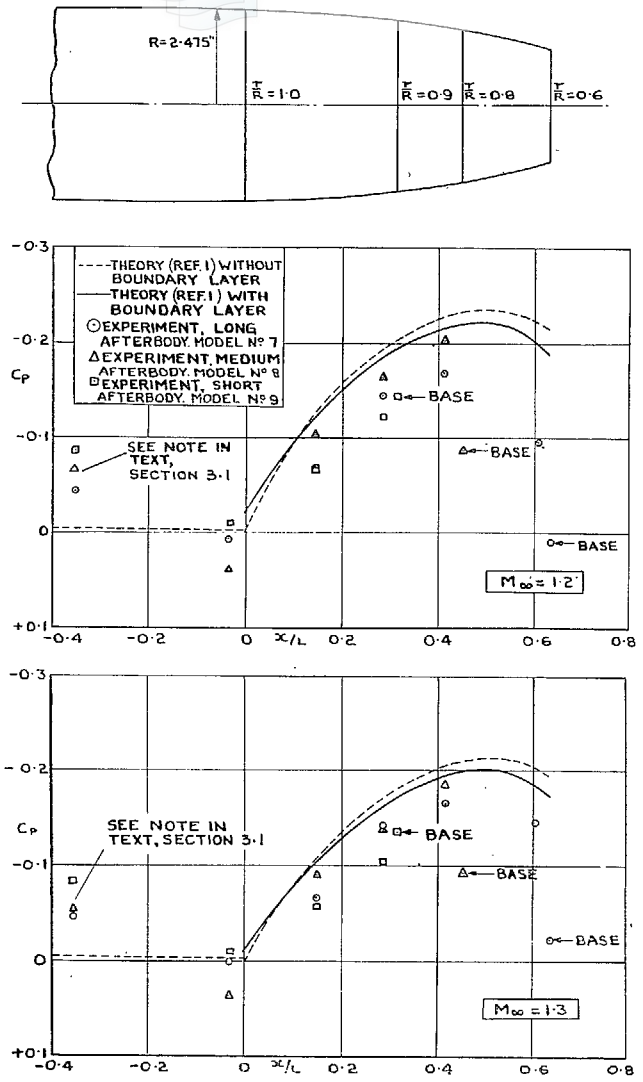

FIG. 9a. Afterbody pressure distribution. $t = 0{\cdot}2$. $M_\infty = 1{\cdot}2$ and $1{\cdot}3$.

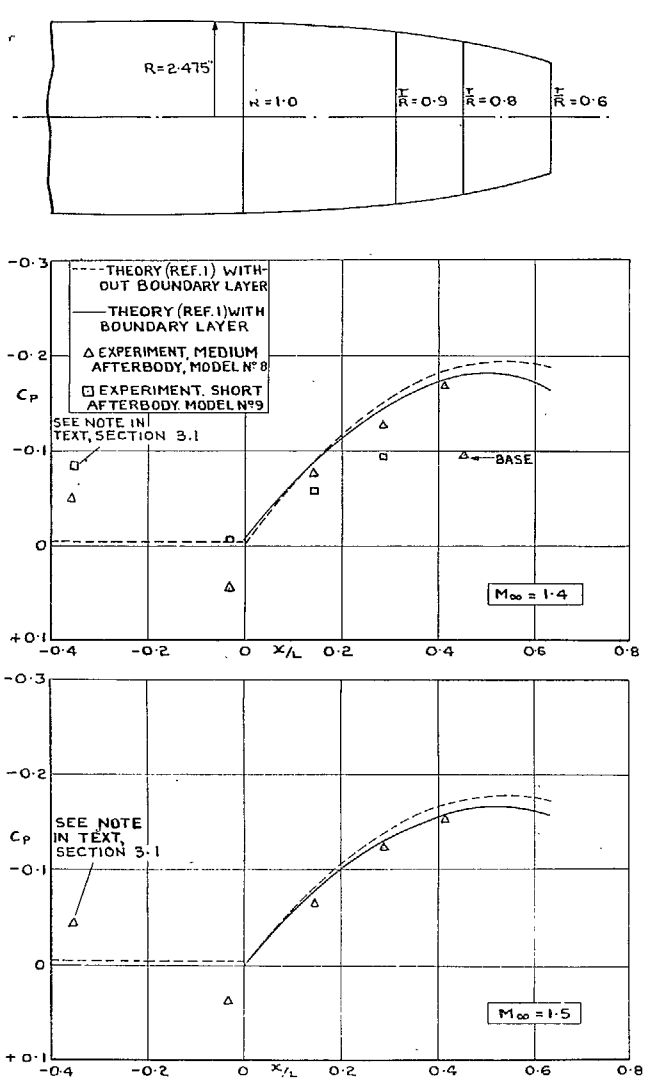

FIG. 9b. Afterbody pressure distribution. $t = 0{\cdot}2$. $M_\infty = 1{\cdot}4$ and $1{\cdot}5$.

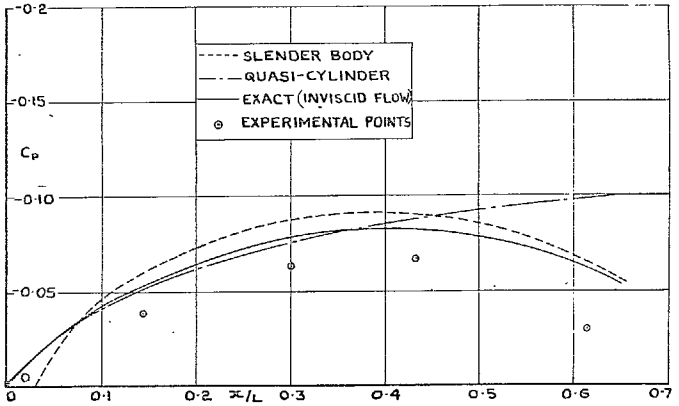

(a) COMPARISON OF MEASURED SURFACE PRESSURE WITH THEORIES.

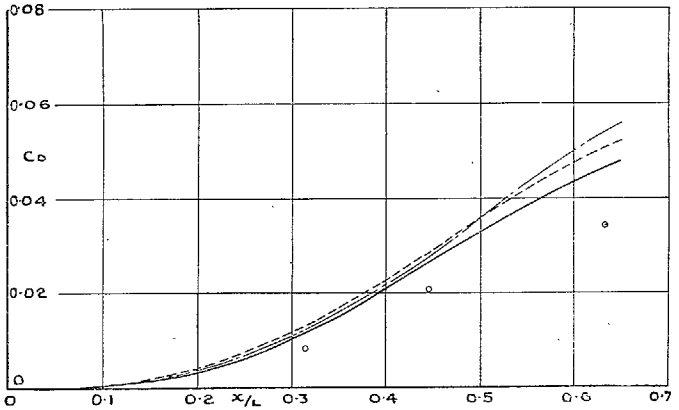

(b) COMPARISON OF MEASURED PRESSURE DRAG WITH THEORIES.

FIG. 10a and b. Comparison of linearised and exact solutions with experiment at $M_\infty = 1{\cdot}2$ for afterbodies where $t = 0{\cdot}1$.

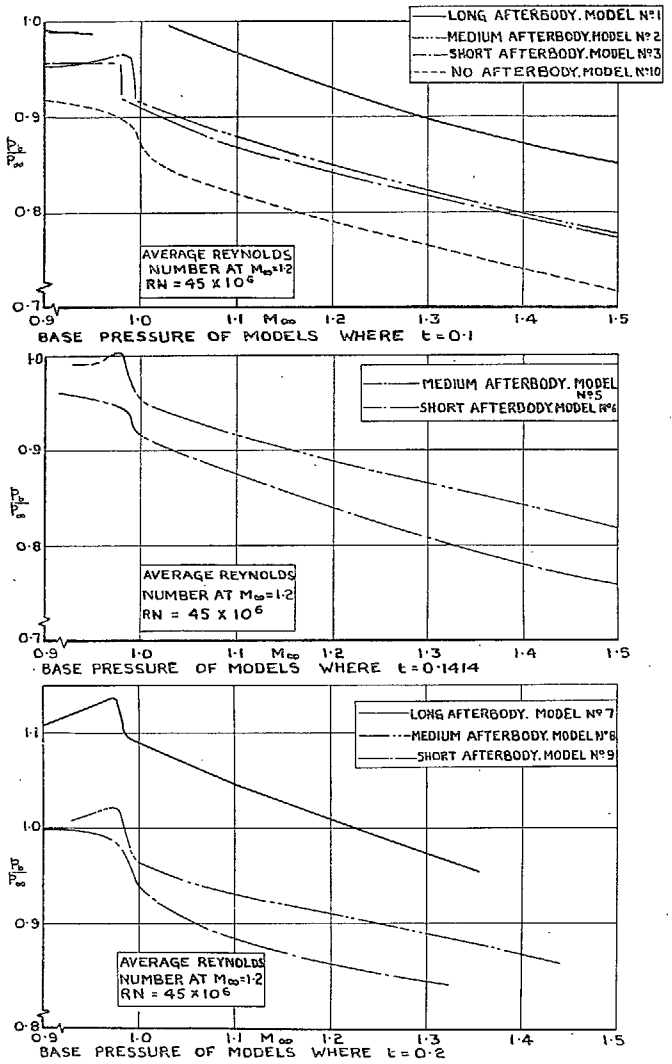

FIG. 11. Variation of base pressure with Mach number.

(85535)

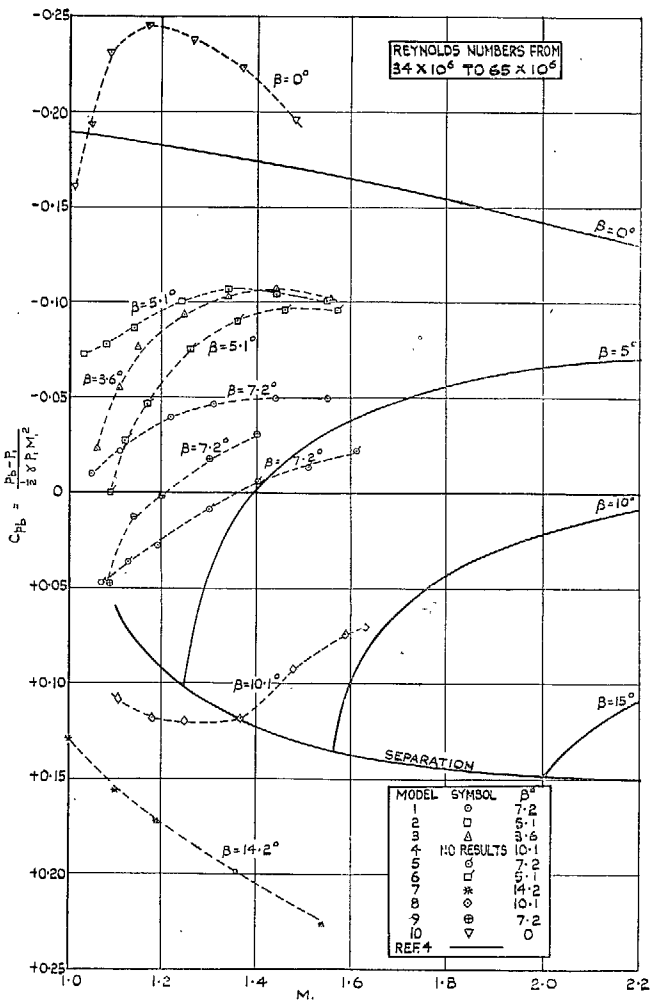

FIG. 12. Comparison between measured base-pressure coefficients and theory suggested in Refs. 3 and 4.

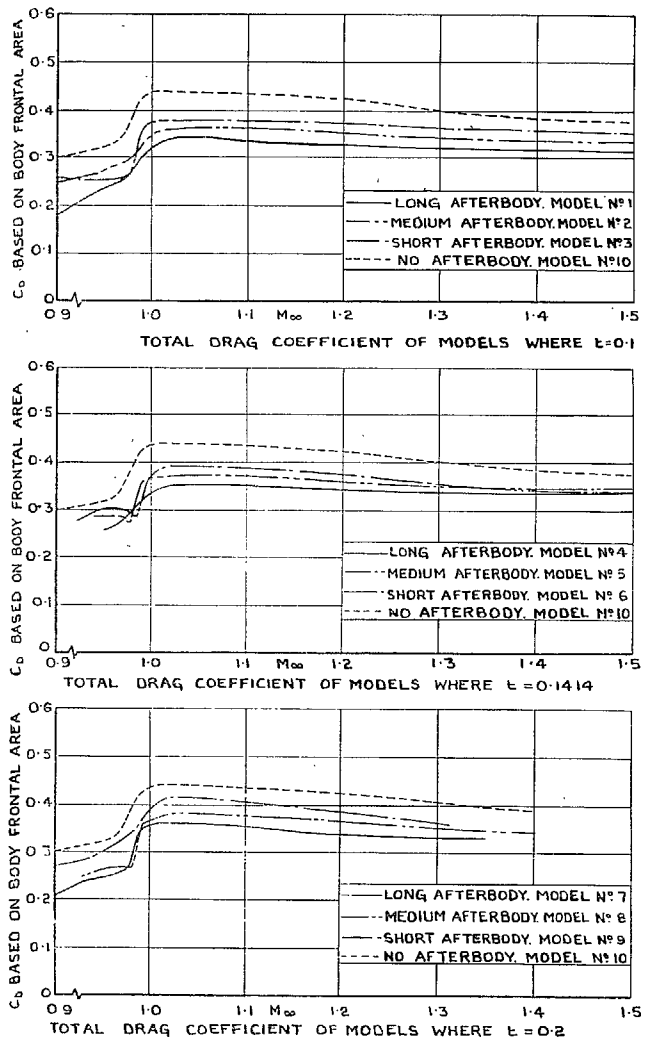

FIG. 13. Variation of measured total drag with Mach number.

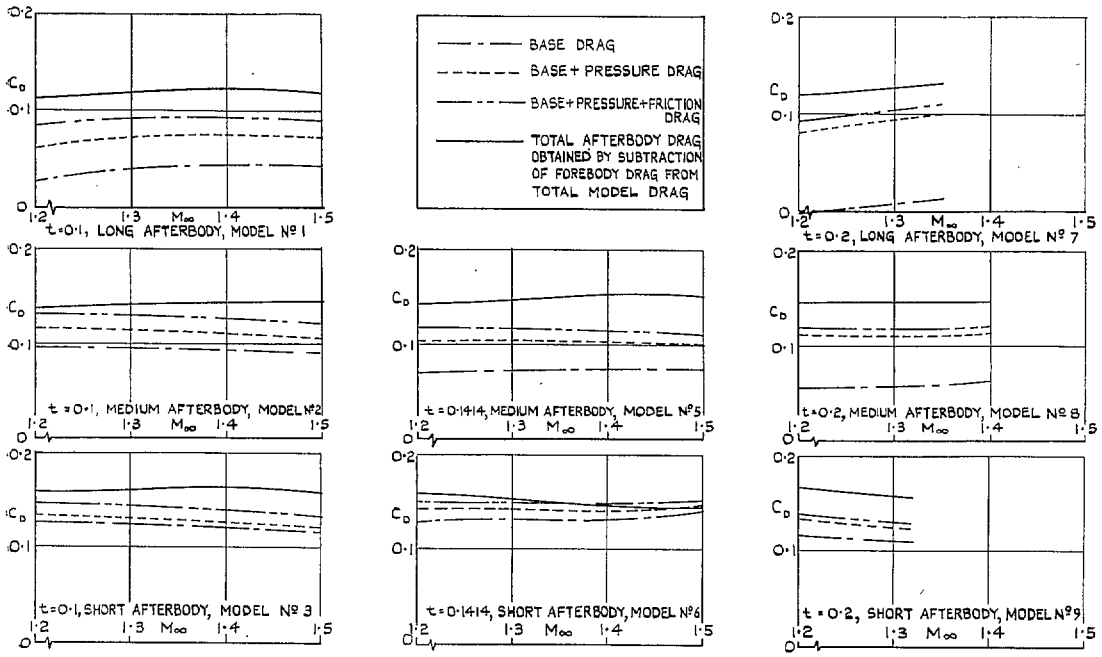

FIG. 14. Breakdown of afterbody drag.

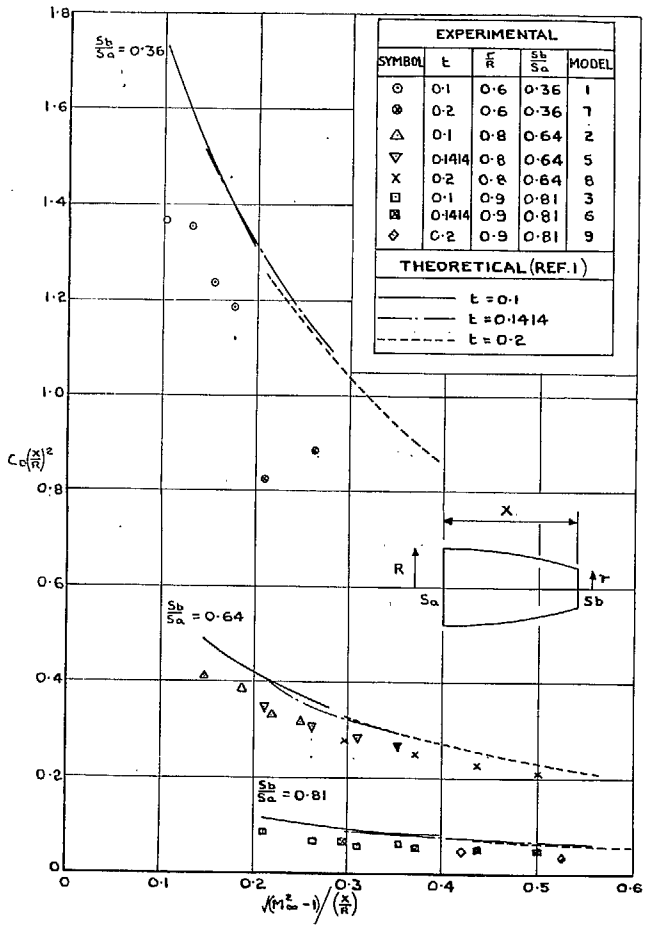

FIG. 15. Afterbody pressure-drag coefficients plotted according to the supersonic similarity law.

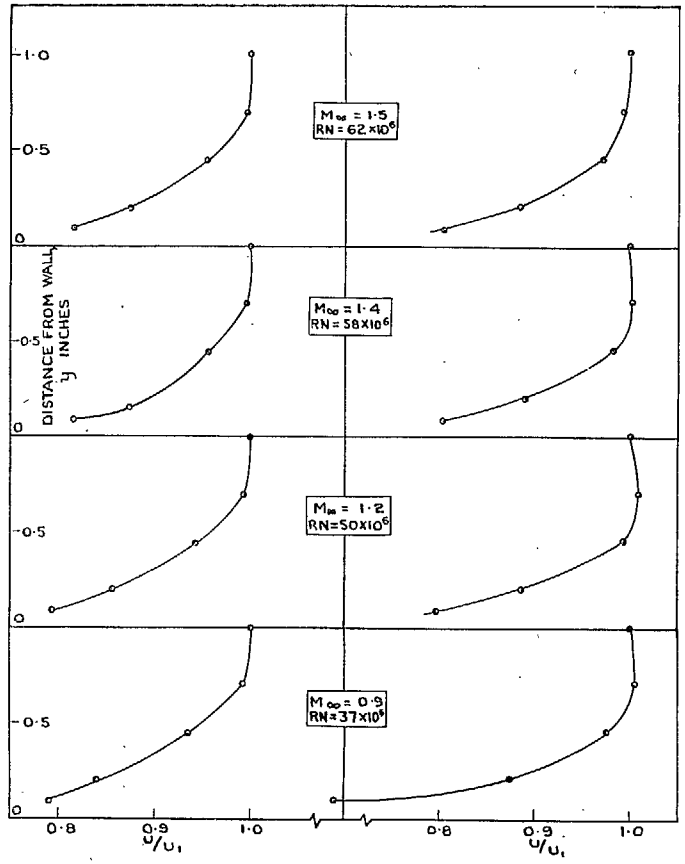

PROFILE MEASUREMENTS ON MODEL 1. PROFILE MEASUREMENTS ON MODEL 3.

FIG. 16. Boundary-layer profiles on models 1 and 3.

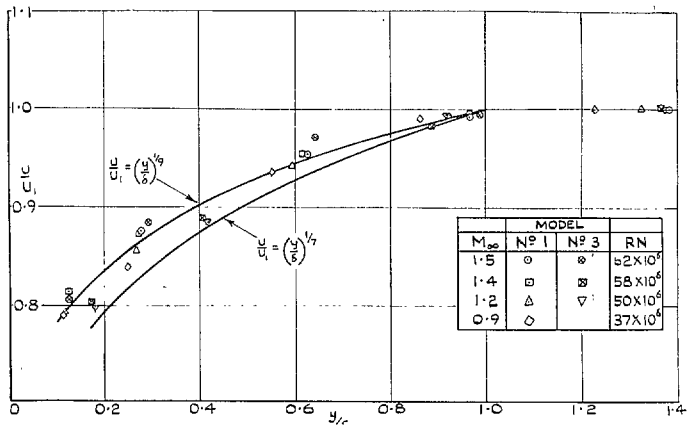

FIG. 17. Comparison between measured and power-law boundary-layer profiles.

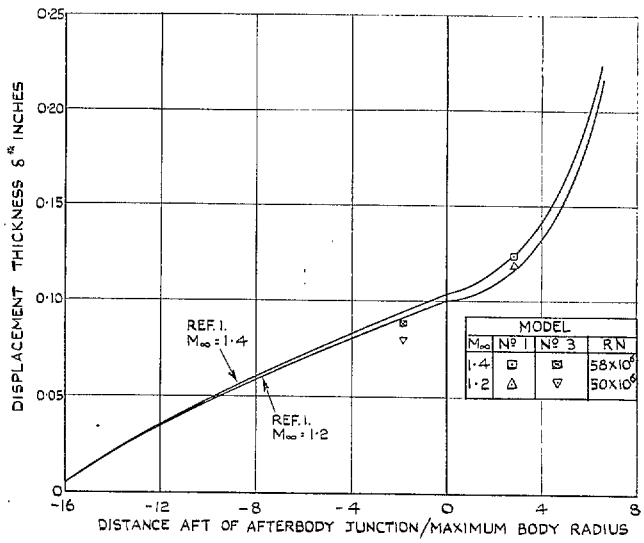

FIG. 18. Comparison between theoretical and measured displacement thickness.

(85535) Wt. 64/1857 K5 11/62 Hw.

Publications of the Aeronautical Research Council

ANNUAL TECHNICAL REPORTS OF THE AERONAUTICAL RESEARCH COUNCIL (BOUND VOLUMES)

1942 Vol. I. Aero and Hydrodynamics, Aerofoils, Airscrews, Engines. 75*s.* (post 2*s.* 9*d.*)
Vol. II. Noise, Parachutes, Stability and Control, Structures, Vibration, Wind Tunnels. 47*s.* 6*d.* (post 2*s.* 3*d.*)

1943 Vol. I. Aerodynamics, Aerofoils, Airscrews. 80*s.* (post 2*s.* 6*d.*)
Vol. II. Engines, Flutter, Materials, Parachutes, Performance, Stability and Control, Structures. 90*s.* (post 2*s.* 9*d.*)

1944 Vol. I. Aero and Hydrodynamics, Aerofoils, Aircraft, Airscrews, Controls. 84*s.* (post 3*s.*)
Vol. II. Flutter and Vibration, Materials, Miscellaneous, Navigation, Parachutes, Performance, Plates and Panels, Stability, Structures, Test Equipment, Wind Tunnels. 84*s.* (post 3*s.*)

1945 Vol. I. Aero and Hydrodynamics, Aerofoils. 130*s.* (post 3*s.* 6*d.*)
Vol. II. Aircraft, Airscrews, Controls. 130*s.* (post 3*s.* 6*d.*)
Vol. III. Flutter and Vibration, Instruments, Miscellaneous, Parachutes, Plates and Panels, Propulsion. 130*s.* (post 3*s.* 3*d.*)
Vol. IV. Stability, Structures, Wind Tunnels, Wind Tunnel Technique. 130*s.* (post 3*s.* 3*d.*)

1946 Vol. I. Accidents, Aerodynamics, Aerofoils and Hydrofoils. 168*s.* (post 3*s.* 9*d.*)
Vol. II. Airscrews, Cabin Cooling, Chemical Hazards, Controls, Flames, Flutter, Helicopters, Instruments and Instrumentation, Interference, Jets, Miscellaneous, Parachutes. 168*s.* (post 3*s.* 3*d.*)
Vol. III. Performance, Propulsion, Seaplanes, Stability, Structures, Wind Tunnels. 168*s.* (post 3*s.* 6*d.*)

1947 Vol. I. Aerodynamics, Aerofoils, Aircraft. 168*s.* (post 3*s.* 9*d.*)
Vol. II. Airscrews and Rotors, Controls, Flutter, Materials, Miscellaneous, Parachutes, Propulsion, Seaplanes, Stability, Structures, Take-off and Landing. 168*s.* (post 3*s.* 9*d.*)

1948 Vol. I. Aerodynamics, Aerofoils, Aircraft, Airscrews, Controls, Flutter and Vibration, Helicopters, Instruments, Propulsion, Seaplane, Stability, Structures, Wind Tunnels. 130*s.* (post 3*s.* 3*d.*)
Vol. II. Aerodynamics, Aerofoils, Aircraft, Airscrews, Controls, Flutter and Vibration, Helicopters, Instruments, Propulsion, Seaplane, Stability, Structures, Wind Tunnels. 110*s.* (post 3*s.* 3*d.*)

Special Volumes

Vol. I. Aero and Hydrodynamics, Aerofoils, Controls, Flutter, Kites, Parachutes, Performance, Propulsion, Stability. 126*s.* (post 3*s.*)
Vol. II. Aero and Hydrodynamics, Aerofoils, Airscrews, Controls, Flutter, Materials, Miscellaneous, Parachutes, Propulsion, Stability, Structures. 147*s.* (post 3*s.*)
Vol. III. Aero and Hydrodynamics, Aerofoils, Airscrews, Controls, Flutter, Kites, Miscellaneous, Parachutes, Propulsion, Seaplanes, Stability, Structures, Test Equipment. 189*s.* (post 3*s.* 9*d.*)

Reviews of the Aeronautical Research Council

1939–48 3*s.* (post 6*d.*) 1949–54 5*s.* (post 5*d.*)

Index to all Reports and Memoranda published in the Annual Technical Reports

1909–1947 R. & M. 2600 (out of print)

Indexes to the Reports and Memoranda of the Aeronautical Research Council

Between Nos. 2351–2449 R. & M. No. 2450 2*s.* (post 3*d.*)
Between Nos. 2451–2549 R. & M. No. 2550 2*s.* 6*d.* (post 3*d.*)
Between Nos. 2551–2649 R. & M. No. 2650 2*s.* 6*d.* (post 3*d.*)
Between Nos. 2651–2749 R. & M. No. 2750 2*s.* 6*d.* (post 3*d.*)
Between Nos. 2751–2849 R. & M. No. 2850 2*s.* 6*d.* (post 3*d.*)
Between Nos. 2851–2949 R. & M. No. 2950 3*s.* (post 3*d.*)
Between Nos. 2951–3049 R. & M. No. 3050 3*s.* 6*d.* (post 3*d.*)
Between Nos. 3051–3149 R. & M. No. 3150 3*s.* 6*d.* (post 3*d.*)

HER MAJESTY'S STATIONERY OFFICE

from the addresses overleaf

Printed and published by
HER MAJESTY'S STATIONERY OFFICE

To be purchased from
York House, Kingsway, London W.C.2
423 Oxford Street, London W.1
13A Castle Street, Edinburgh 2
109 St. Mary Street, Cardiff
39 King Street, Manchester 2
50 Fairfax Street, Bristol 1
35 Smallbrook, Ringway, Birmingham 5
80 Chichester Street, Belfast 1
or through any bookseller

Printed in England

S.O. Code No. 23–3290